Biosensors and Bioelectronics 191 (2021) 113387

Contents lists available at ScienceDirect

Biosensors and Bioelectronics

journal homepage: www.elsevier.com/locate/bios

Enzyme-free impedimetric biosensor-based molecularly imprinted polymer for selective determination of L-hydroxyproline

Whitchuta Jesadabundit [a], Sakda Jampasa [b], Kanitha Patarakul [c], Weena Siangproh [d,*], Orawon Chailapakul [a,e,**]

[a] Electrochemistry and Optical Spectroscopy Center of Excellence (EOSCE), Department of Chemistry, Faculty of Science, Chulalongkorn University, Pathumwan, Bangkok, 10330, Thailand
[b] Institute of Biotechnology and Genetic Engineering, Chulalongkorn University, Patumwan, Bangkok, 10330, Thailand
[c] Department of Microbiology, Faculty of Medicine, Chulalongkorn University, Pathumwan, Bangkok, 10330, Thailand
[d] Department of Chemistry, Faculty of Science, Srinakharinwirot University, Sukhumvit 23, Wattana, Bangkok, 10110, Thailand
[e] National Center of Excellent of Petroleum, Petrochemicals, and Advanced Materials, Chulalongkorn University, Phayathai Road, Pathumwan, Bangkok, 10330, Thailand

ARTICLE INFO

Keywords:
L-hydroxyproline
Molecularly imprinted polymer
Electrochemical impedance spectroscopy
Non-enzymatic sensor
Bone diseases

ABSTRACT

This study first reported enzyme-free impedimetric biosensor-based molecularly imprinted polymers for selective and sensitive determination of L-hydroxyproline (L-hyp), a biomarker for the early diagnosis of bone diseases. In recent study, utilizing a single 3-aminophenylboronic acid (3-APBA) to create imprinted surfaces could result in a strong interaction and difficulty in removal of a template molecule. Hence, a mixture of monomer solution containing 3-APBA and o-phenylenediamine (OPD) in the presence of the L-hyp molecule was co-electropolymerized onto the screen-printed electrode using cyclic voltammetry (CV) to eradicate this mentioned limitation. The detection principle of this sensor is relied on alteration of mediator's charge transfer resistance (R_{ct}) that could be obstructed by L-hyp occupied in imprinted surface. The successfully fabricated biosensor was explored by scanning electron microscopy (SEM), Fourier-transform infrared spectroscopy (FTIR), and confocal scanning microscopy. Furthermore, the effect of polymer composition on the R_{ct} response was systematically investigated. The result exhibited that the mixture of monomers could provide the highest change of R_{ct} due to high selectivity from esterification of 3-APBA and from hydrogen bond of OPD surrounding the template. The sensor showed a significant increase in R_{ct} in the presence of L-hyp, whereas no observable resistance change was detected in the absence thereof. The calibration curve was obtained in the range from 0.4 to 25 μg mL^{-1} with limits of detection ($3SD_{blank}$/Slope) and quantification ($10SD_{blank}$/Slope) of 0.13 and 0.42 μg mL^{-1}, respectively. This biosensor exhibited high selectivity and sensitivity and was successfully applied to determine L-hyp in human serum samples with satisfactory results.

1. Introduction

Bone resorption is a part of the bone metabolism process associated with the removal of old or damaged bone by osteoclast cells. The bone metabolism can be imbalanced by some bone disorders such as osteoporosis, rheumatoid arthritis, and bone cancer (Feng and McDonald, 2011; Kotwal et al., 2019). Over several decades, the Dual energy x-ray absorptiometry (DXA) and Radiological examination have been generally used to diagnose the bone diseases; however, these techniques are not reliable until the apparent change of 30%–40% in the bone density is detected (Kontturi et al., 1974; Russell et al., 2001; Wasserman et al., 2017). Consequently, the determination of a specific biomarker linked with bone diseases has become an essential part of an early prognosis and confirmation.

L-hydroxyproline (L-hyp) is a nonessential amino acid and non-proteinogenic compound that differs from proline by its hydroxyl group, produced via post-translational of proline, at the γ carbon atom (Srivastava et al., 2016). To date, there is a report describing the

* Corresponding author. Electrochemistry and Optical Spectroscopy Center of Excellence (EOSCE), Department of Chemistry, Faculty of Science, Chulalongkorn University, 254 Phayathai Road, Pathumwan, Bangkok, 10330, Thailand.
** Co-corresponding author. Department of Chemistry, Faculty of Science, Srinakharinwirot University, Sukhumvit 23, Wattana, Bangkok, 10110, Thailand.
E-mail addresses: weena@g.swu.ac.th (W. Siangproh), corawon@chula.ac.th (O. Chailapakul).

https://doi.org/10.1016/j.bios.2021.113387
Received 21 April 2021; Received in revised form 25 May 2021; Accepted 28 May 2021
Available online 3 June 2021

degradation of bone collagen in which L-hyp can be released during the process. Additionally, 90% of the degradation process is metabolized in the liver (Seibel, 2005). Hence, based on this previous study, the analysis of L-hyp in a biological fluid would be the simplest way to sensitively and rapidly detect an early stage of bone diseases (Ahmed et al., 2015; Kontturi et al., 1974).

So far, numerous methods have been established for L-hyp determination in biological fluids, tissues, and food products. These developed techniques include colorimetric methods (Jamall et al., 1981; Woessner, 1961), high-performance liquid chromatography (HPLC) (Bianchi and Mazza, 1995; Messia et al., 2008; Ren et al., 2017; Teerlink et al., 1989; Zheng et al., 2018), gas chromatography (Delport et al., 2004), micellar electrokinetic chromatography (MEKC) and capillary electrophoresis with electrochemiluminescence (Liang et al., 2005; Xu et al., 2009), and MEKC with laser-induced fluorescence (Chan et al., 1993; Dong et al., 2012). Each approach has its well-known performance in terms of high sensitivity and selectivity. However, some drawbacks such as complicated equipment, high maintenance cost, a requirement of derivatization and sample preparation, lots of reagents, and long-time analysis still exist.

Alternatively, electrochemical technique has gained considerable interest for the development of simple, portable, and rapid detection method because of its high sensitivity and selectivity (Azevedo et al., 2019; Babadi et al., 2019; Bi et al., 2016; Govindasamy et al., 2019). Recently, the first enzymatic electrochemical biosensor for L-hyp determination using a screen-printed carbon electrode (SPCE) was proposed (Sakamoto et al., 2015). In this reported platform, two enzymes and ferrocene carboxylic acid were used to specifically alter L-hyp into electroactive species and to directly indicate the presence and absence of target analyte, respectively. However, this introduced troublesome platform requires a complicated process and the use of specific enzymes, which is unstable in harsh working conditions or in a longer-time storage. To overcome this challenge, developing a novel methodology which is enzyme-free and can be portable for L-hyp determination, is therefore necessary.

Molecularly imprinted polymer (MIP) has received great attention and is now rapidly growing for the fabrication of electrochemical biosensors (Sheej Ahmad, 2018). MIP offers the complementary shape, size, and chemical fit for binding a target molecule on the generated polymeric film with high selectivity and specificity (Mujahid and Dickert, 2016). Therefore, the present study aimed to first develop MIP-based electrochemical impedimetric biosensor for enzyme-free sensitive and selective L-hyp determination. The MIP capture surface was created by co-electropolymerization of a monomer solution containing 3-aminophenylboronic acid and *o*-phenylenediamine (*o*-PD) in the presence of L-hyp molecule using a user-friendly and environmental cyclic voltammetry (CV) technique. Additionally, this proposed platform was successfully applied to determine L-hyp in human serum without the necessity of the sample pretreatment step. These obtained results indicated that this proposed device has a great efficiency to be used as an alternative tool for the clinical diagnosis of an early stage of bone diseases.

2. Experimental

2.1. Chemicals and apparatus

The details of chemicals and apparatus used for MIP sensor preparation, L-hyp detection and also analytical performance study were all specified in supporting information (SI) section 1 and 2, respectively.

2.2. Fabrication of the SPCE

The screen-printing technology was applied to fabricate the SPCE. The electrode pattern was designed using the Adobe Illustrator program, and a polyvinyl chloride (PVC) sheet with a thickness of 0.15 mm from IDee-craft Co. Ltd. (Bangkok, Thailand) was used as an electrode substrate. The screen printing method and conductive ink used in this work were mentioned in section 3 of experimental, SI.

2.3. Preparation of the MIP and non-imprinted polymer (NIP) biosensors

In Fig. 1, the preparation process of MIP was demonstrated step by step. First, a mixture solution of 7 mM aminophenylboronic acid, 3 mM *o*-PD, and 3 mM L-hyp in 0.1 M phosphate buffer of pH 7.4 was dropped on the electrode surface, followed by a co-electropolymerization process using CV as explained in section 1, SI. The potential range was scanned from 0 to +1.2 V with a scan rate of 50 mV s^{-1} for 15 cycles. Fig. S1 presents the obtained cyclic voltammograms. After the polymerization process, the modified electrodes were then thoroughly rinsed with MilliQ water, followed by immersing in 0.3 M H_2SO_4 for 15 min to extract the L-hyp from the polymeric film. The specific cavities on the MIP surface were eventually created in the final step, and this fabricated biosensor was ready to use for the analysis of L-hyp. The same condition was also applied to prepare a NIP, except that L-hyp was excluded from the polymerization solution.

2.4. Electrochemical L-hyp determination

For the detection of L-hyp, the prepared MIP or NIP sensors were incubated with 50 μL of L-hyp solution for 10 min, followed by rinsing with MillQ water to eradicate the L-hyp molecule surplus. The presence and absence of L-hyp were monitored by detecting the change in electrochemical resistance at the electrode interface using EIS technique in 5 mM $[Fe(CN)_6]^{3-/4-}$ redox probe. EIS was applied to conduct both qualitative and quantitative analysis, and the applied potential was +0.1 V (frequency range between 0.01 and 100,000 Hz with 57 frequencies distributed logarithmically). The EIS data were reported as a difference of charge transfer resistance (ΔR_{ct}) between the presence and absence of target analyte. Additionally, CV was also used to further verify the presence and absence of L-hyp. For CV technique, the analysis was conducted by using the scanning potential ranging from −1.0 to +1.2 V with a scan rate of 50 mV s^{-1}. Fig. 1 illustrates the detection procedure.

2.5. Sample preparation

Human serum was taken from healthy patient and used without purification process. Thereafter, the aliquots (50 μL) of sample were then spiked with the designated concentrations of L-hyp and subsequently diluted with 0.1 M phosphate buffer to the final volume of 500 μL. By using these specified conditions, the analysis can be conducted without a further pretreatment step.

3. Results and discussion

3.1. Characterization of the MIP sensor

To characterize the successful formation of MIP, the Laser scanning confocal microscopy (LSCM) was used to verify the topology change on various electrode surfaces. From the obtained image in Fig. 2, the 3D profile roughness (Ra) was analyzed by scanning through the focus area. As depicted in Fig. 2A, the bare carbon provided blue areas indicating stacked surfaces of carbon sheets with an average roughness of 3.206 μm. Meanwhile, the electrode surface after the polymerization step (Fig. 2B) presented a green image with decreasing value of roughness to 2.599 μm due to coating of polymer. After template removal step (Fig. 2C), the scanning image turned to a dispersing of blue dots with an increment of surface roughness to 2.873 μm, which obviously supported the successful removal of template molecules and formation of the MIP cavities on the electrode surface. All these results confirmed the successful fabrication of the MIP sensor in a-step-by-step fashion. The

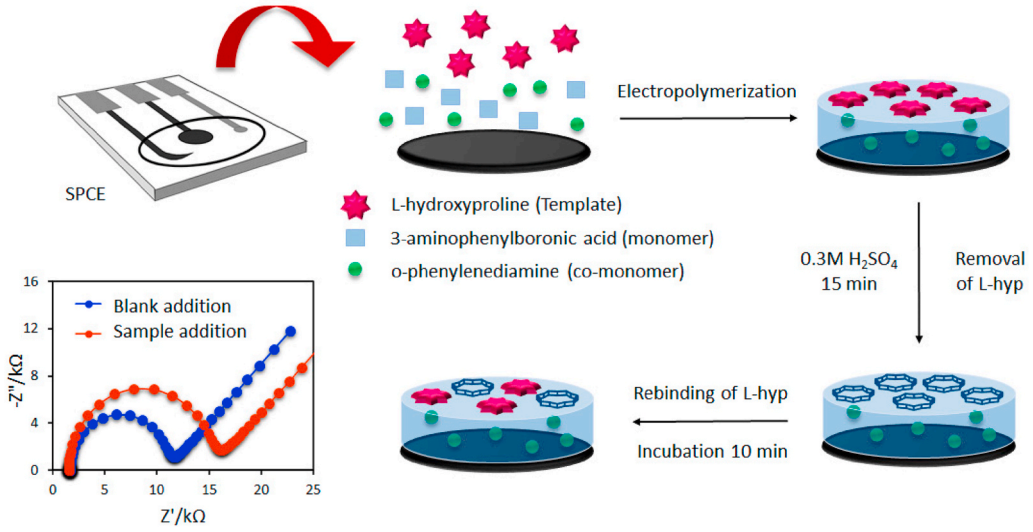

Fig. 1. Schematic illustration of the fabrication and operation of MIP/SPCE biosensor.

prepared MIP sensor was further characterized by FTIR and SEM to confirm the polymerization and formation of imprinted cavities. The obtained results with its description can be found in SI, section 5.

To investigate the electrochemical behavior of the fabricated biosensors, the modified SPCEs were characterized via CV using a 5 mM $[Fe(CN)_6]^{3-/4-}$ (Fig. 2D). With the bare carbon electrode (SPCE), a reversible redox peak in a cyclic voltammogram was detected. However, after the electropolymerization process (MIP/SPCE), a significant decrease in the current response was observed. This result can be explained by the hindering effect of the generated polymeric film on the electrode surface, resulting in the diffusion and electron transfer of the redox probe applied toward the electrode interface. Additionally, a possible explanation is that the current response could be affected by an entrapment of amino acids inside the polymeric layer, which consequently resulted in the declining signal. As expected, the peak current was increased after the removal of the template molecule. This improved signal would be caused by the generation of the specific cavities on the polymeric surface, enhancing an electroactive surface area. Based on these obtained results, the diffusion and redox reaction of $[Fe(CN)_6]^{3-/4-}$ would be much more enhanced. Upon the MIP was incubated with L-hyp, the low-current response was observed. Additionally, the redox peak of $[Fe(CN)_6]^{3-/4-}$ shifted positively. These obtained results may be due to the rebinding of L-hyp on the electrode surface; consequently, the obstruction of the electrode surface was generated, resulting in poor electrical conductivity and accessibility of the sensor and redox probe used, respectively.

Additionally, the successful fabrication of MIP was verified by EIS, and the results were consistent with those achieved by the CV study. Fig. 2E shows that the bare carbon electrode (SPCE) displayed low resistance with an R_{ct} of 6.79 kΩ, indicating high-electron transfer capability. The polymerization then caused an increase in R_{ct} of 14.6 kΩ as a result of the non-conducting polymeric film generated on the electrode surface that obstructs the electron transfer. However, after the removal of the template, the impedance once again decreased to 9.89 kΩ, indicating the formation of unoccupied cavities. The holes among polymer molecule arrangements help the redox probe to permeate and deliver electrons easily. As expected, after the rebinding of the substrate, the R_{ct} response value dramatically increased to 13.5 kΩ. This was due to the shielding effect on the sensor surface created by occupied L-hyp.

To investigate the relationship between R_{ct} and the heterogeneous electron transfer rate constant (K_{et}), equation (1) was applied for each electrode calculation (Bradbury et al., 2010; Jampasa et al., 2016).

$$K_{et} = \frac{RT}{n^2F^2R_{ct}AC_{redox}} \quad (1)$$

A is the geometrical area of the electrode surface, and C_{redox} is the concentration of the $[Fe(CN)_6]^{3-/4-}$. From the calculation, K_{et} was found to be at 4.77×10^{-5}, 2.81×10^{-5}, 3.27×10^{-5}, and 2.22×10^{-5} cm s^{-1} for the unmodified SPCE, MIP/SPCE after polymerization, MIP/SPCE after removal, and MIP/SPCE after rebinding template, respectively. These obtained values reasonably correspond to the charge transfer resistance of each electrode. The evidence here therefore verified the successful modification of the MIP sensor.

3.2. Optimization of experimental conditions

To improve the sensitivity of MIP/SPCE, the number of electropolymerization cycle, the concentration of L-hyp template molecule, 3-APBA monomer, *o*-PD co-monomer, the rebinding time, and removing time were systematically optimized by using different electrodes. All plotted data in the graph were from the average of three repeated measurements (n = 3). The error bars seen in the graph were used to represent standard deviation (SD) of each Fig. 5 data, and it was found that the SD and %RSD values of less than 0.3 and 7.39% were achieved, respectively. These results were acceptable in accordance with AOAC method. Fig. S5A shows the ΔR_{ct} of 1 μg mL^{-1} L-hyp at the MIP sensor prepared with different numbers of electropolymerization cycle. In Fig. S5A, the progressive increment in ΔR_{ct} was observed; however, these responsive values decreased with rising the electropolymerization cycle. The film prepared at 15 cycles offered the highest sensitivity. Based on this result, it can be concluded that less cycle number caused a thin layer of polymer membrane, which is not sufficient for the formation of specific cavities and binding sites. So, it provided a negligible change on the resistive response. After more cycles (more than 15 cycles), the signal was remarkably declined because this condition could increase the thickness of the polymer. The templates embedded in the polymer layer are hard to be removed for the cavities fabrication, subsequently resulting in low capacity of detection. Also, the 3-APBA and OPD are non-conductive polymers that their thickness can provide the high background resistance and reduce the sensitivity (Li et al., 2012; Zhao et al., 2020). Thus, 15 cycles of the electropolymerization process were therefore chosen for the next experiments.

Because template concentration is another parameter that enormously affects the number and complementary shape of imprinted cavities, the MIP solution with different L-hyp template concentrations was subsequently optimized. Fig. S5B shows that the impedance

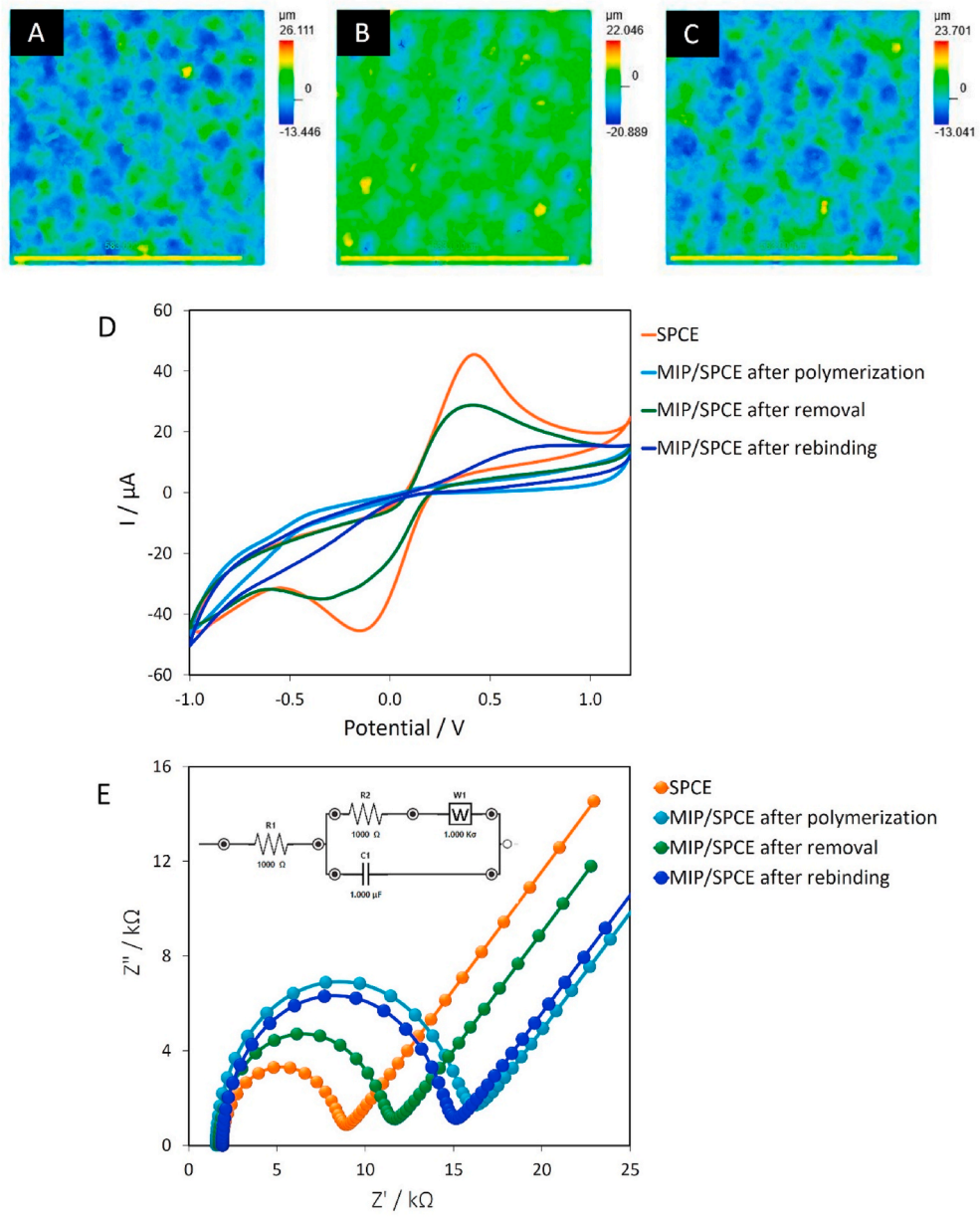

Fig. 2. Confocal laser scanning microscopy images of the bare carbon electrode (A), electrode after polymerization (B), and after template removal process to fabricate MIP (C). Characterization of the MIP/SPCE sensor: Cyclic voltammograms (D) and EIS Nyquist plot (E) using 5 mM $K_3[Fe(CN)_6]/K_4[Fe(CN)_6]$ in 100 mM KCl.

gradually increased with increasing the concentration of template molecules and eventually reached the greatest value at 3 mM of L-hyp. The ΔR_{ct} response was then declined at a higher concentration of L-hyp since a large number of template molecules were embedded into the MIP surface, causing the difficulty of template removal after an imprinting process (Zhu et al., 2018). The evidence here therefore suggested that the optimal condition for this parameter was 3 mM of template concentration.

Because of a covalent bond formation of 3-APBA toward the target molecule via boronate ester (Mujahid and Dickert, 2016), the effect of 3-APBA concentration on impedimetric response was studied. Fig. S5C shows that the resistance of the electrode surface progressively increased within the concentration ranging from 3 to 7 mM and then reached a maximum value at 7 mM. Nevertheless, at conditions above these limits, the decrease in electrode resistance was observed. This considerable decrease is due to an increment of boronic acid functional groups on the polymer surface that induce more template immobilization and formation (Luo et al., 2017); thus, the diffusion of analyte on the electrode surface was obstructed. Thus, the concentration of 7 mM 3-APBA was selected as the optimal condition.

Further, the concentration of *o*-PD was investigated as illustrated in Fig. S5D. Similarly, the enhanced impedance was detected when the concentrations of *o*-PD ranging from 1 to 3 mM were used. However, at any concentrations above 3 mM, the responsive resistance was remarkably decreased. It can be concluded, based on these achieved results, that the optimum mole ratio of 3-APBA, *o*-PD, and L-hyp was 2:1:1 mol. In addition, the comparison of using single and two monomers were studied by investigation of obtained resistance after sample incubation on prepared MIPs: 3-APBA, OPD, and mixing of 3-APBA and OPD. This evidence confirmed the high recognition capability of the hybrid monomer, which is a consequence of their highly specific binding site and geometrical selectivity initiated by esterification of 3-APBA and hydrogen bond of OPD, respectively as described in SI, section 6.

In Figs. S5E and S5F, the influence of rebinding and removing time

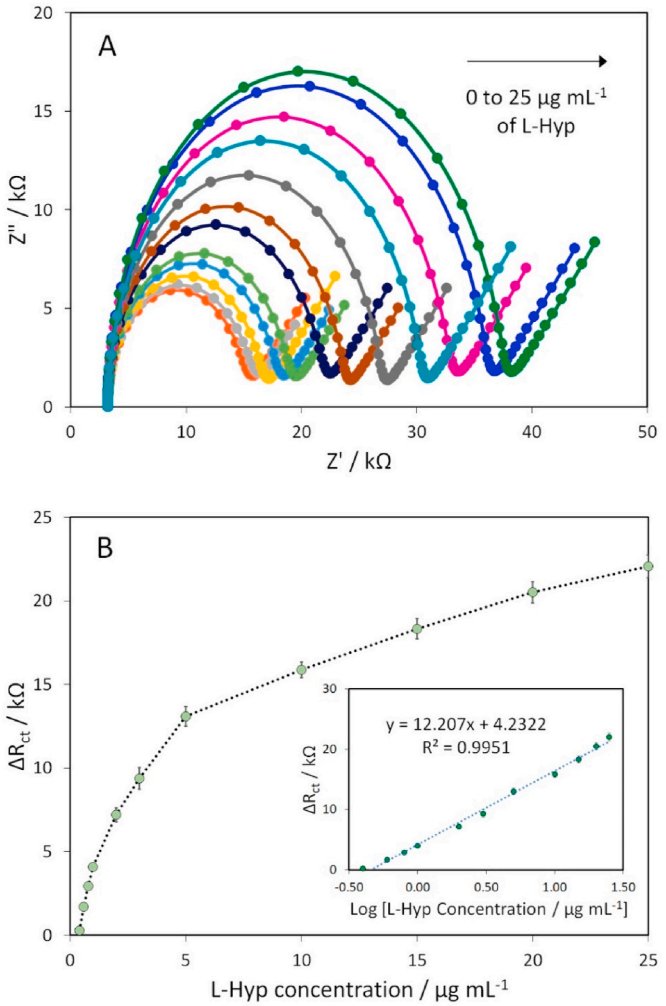

Fig. 3. The impedimetric responses of the MIP/SPCE after incubating with various L-hyp concentrations of 0.4, 0.6, 0.8, 1, 2, 3, 5, 10, 15, 20, 25 μg mL^{-1} (A). The plot of charge transfer resistances and concentrations (B) and inset (B) is the plot of ΔRct against logarithmic of L-hyp concentration.

on the ΔR_{ct} response was examined. Both resistances initially increased with the elongation of time and then attained equilibrium at 10 and 15 min for the rebinding and removing time, respectively. In the case of binding, it is presumed that the longer accumulation raises the amount of L-hyp absorbing on MIP. However, in the case of the plateau response, a possible description could be that the saturation of the electrode surface is achieved at conditions above these limits (Shen et al., 2018). Similarly, enhancing removing time also influenced the efficiency of template removal.

3.3. Analytical performance

The analytical performance of MIP/SPCE was investigated after achieving the optimal conditions. The changed ΔR_{ct} of the proposed biosensor after incubating with various concentrations of L-hyp ranging from 0 to 25 μg mL^{-1} was accessed (Fig. 3A). In Fig. 3B, the ΔR_{ct} was plotted against logarithmic L-hyp concentration, and the result revealed that good linearity was achieved from 0.4 to 25 μg mL^{-1}. The linear regression equation was ΔR_{ct} (kΩ) = 12.207 C (μg mL^{-1}) + 4.2322 (R^2 = 0.9951) (Fig. 3B (inset)). The limits of detection (LOD) and quantification (LOQ) were calculated to be 0.13 and 0.42 μg mL^{-1} using the equations of $3S_b/m$ and $10S_b/m$, respectively. S_b is the standard deviation of blank measurement (n = 7) and m is the slope of the calibration curve. Comparison of analytical performance between the developed and previously reported methods related to electrochemical technique for L-hyp determination in biological samples was discussed in SI, section 8.

In term of stability and reproducibility, the experimental details and results are also shown in SI section 9 and Fig. S6, respectively.

3.4. Influence of interferences

The commonly found interferences in human serum such as alanine, glycine, histidine, lysine, proline, uric acid, creatinine, and ascorbic acid were evaluated to further access the selectivity and specificity of the created L-hyp biosensor. The mixture solution of L-hyp (0.5 μg mL^{-1}) and other interferences were prepared separately. In Fig. 4, the ΔR_{ct} value was insignificantly changed when the L-hyp standard solution was mixed with a 100-fold greater concentration of alanine, glycine, histidine, lysine, and proline. Additionally, the impedance response was also unaffected by the 10-fold of creatinine, uric acid, and ascorbic acid. All these examined concentrations covered the concentration range of the interferences that might exist in the real sample. Further, the error of ΔR_{ct} was found to be less than 5%, indicating high reproducibility. As expected, the NIP electrode could barely interact with all analytes. Based on these results, it can be therefore concluded that the high selectivity achieved in this study was from the specific cavities caused by complementary size, shape, and functionality.

To further confirm the specificity of this proposed biosensor, the binding affinity of MIP toward L-hyp and other amino acids including proline, lysine, and glycine was investigated using the calibration data (Chen et al., 2018) as provided in SI section 10.

3.5. Determination of L-hyp in human serum samples

Human serum samples obtained from healthy patients were employed in the entire process to test the applicability of the proposed sensor for real sample analysis. These samples were spiked with different L-hyp concentrations (0, 1, 5, and 20 μg mL^{-1}) and tested after incubation on MIP surface, resulted in the increase of resistance signal as shown in Fig. 5. In Table 1, the reported concentrations were the average of 3 repeated measurements of each spiked human serum sample. The original concentration of L-hyp in the non-spiked sample ranged from 0.7 to 1.55 μg mL^{-1} which was the normal range of L-hyp for healthy human serum. The found L-hyp concentrations were compared with standard HPLC-UV technique to confirm accuracy and precision of this proposed sensor. The results exhibited that the concentrations of L-hyp achieved from both detection methods were in good agreement. A paired t-test at 95% confidence interval is accomplished using this developed method. The t-calculated value of 1.565 is lower than 4.303, the t-critical value, thereby obviously indicating that there is no significant difference between the established and standard technique. Also, the %recovery and %RSD were found in the range from 99.72 to 103.34 and from 2.14 to 4.62, respectively, further confirming the sensor's accuracy and precision.

4. Conclusions

An enzyme-free impedimetric biosensor-based on MIP for bone disease biomarker, L-hyp, was successfully developed and applied to selectively detect human serum samples with differently spiked L-hyp concentrations. Charge transfer resistance (R_{ct}) was significantly increased only in the presence of the correct analyte. For the investigation of binding affinity, the developed biosensor showed an excellent specificity toward the L-hyp molecule rather than the other similar structure amino acids confirmed with the K_d value of 27.56 ± 1.77 μM. Under the optimal conditions, the analytical performance was examined, and it was found that the developed biosensor exhibited a linear relationship between 0.4 and 25 μg mL^{-1}. By using this platform, the LOD and LOQ values of 0.13 and 0.42 μg mL^{-1} were obtained,

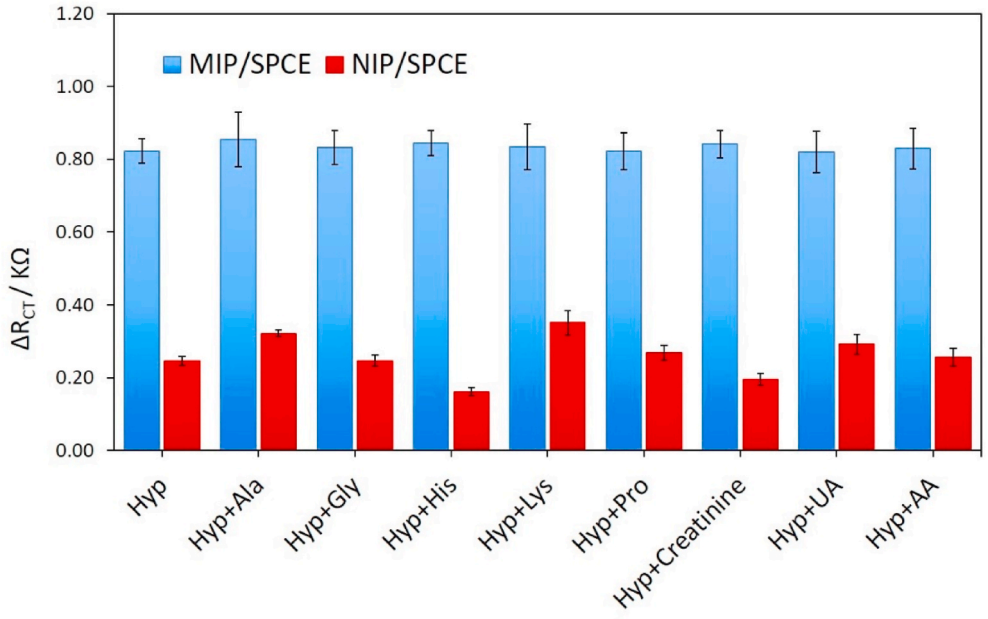

Fig. 4. The selectivity test of MIP and NIP electrodes toward L-hyp and its molecularly similar structures.

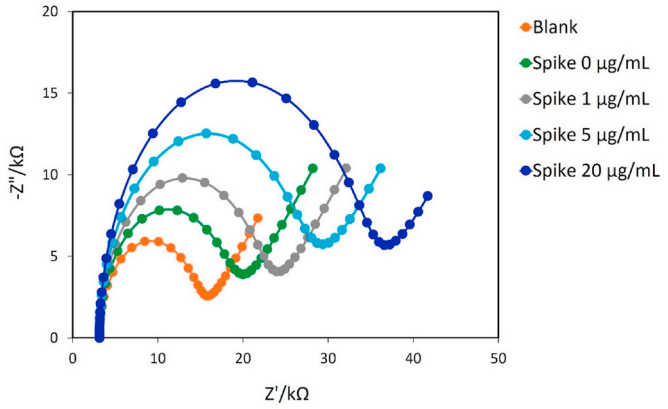

Fig. 5. Nyquist plots of the MIP/SPCE biosensor for the analysis of human serum samples with differently spiked L-hyp concentrations (0, 1, 5, and 20 μg mL^{-1}) using the optimal conditions.

Table 1
Comparison of the achieved results between the proposed and standard HPLC-UV method for the quantification of L-hyp (n = 3).

Sample	Added (μg/mL)	Found (μg/mL)		% Recovery	% RSD
		HPLC-UV	Developed biosensor		
Human serum	0	0.91 ± 0.09	0.98 ± 0.05	–	4.62
	1	2.01 ± 0.01	2.01 ± 0.06	103.34	2.75
	5	5.87 ± 0.16	5.97 ± 0.13	99.72	2.14
	20	21.07 ± 0.17	21.34 ± 0.93	101.79	4.37

respectively. These obtained values cover the concentration interval of L-hyp that can be found in healthy humans and patients with an early stage of bone diseases. To the best of our knowledge, this is the first non-enzymatic electrochemical biosensor for direct L-hyp determination in a biological fluid. This fabricated biosensor offers several advantages including simple operation, high selectivity, and long-term stability for up to 18 days. Additionally, by using this developed method, sample pretreatment steps are not required, thus reducing the analysis time. Hence, it can be assumed that this fabricated L-hyp biosensor has a great potential to be applied in a clinical field as an alternative tool to access the risk development of bone diseases and also symptom tracking.

CRediT authorship contribution statement

Whitchuta Jesadabundit: Conceptualization, Methodology, Investigation, Writing – original draft. **Sakda Jampasa:** Conceptualization, Supervision, Writing – review & editing. **Kanitha Patarakul:** Validation, Methodology. **Weena Siangproh:** Supervision, Writing – review & editing. **Orawon Chailapakul:** Conceptualization, Visualization, Project administration, Supervision, Funding acquisition.

Declaration of competing interest

The authors declare that they have no known competing financial interests or personal relationships that could have appeared to influence the work reported in this paper.

Acknowledgment

O.C. would like to thank the National Research Council of Thailand (NRCT) for supporting. W.J. wish to thank the Science Achievement Scholarship of Thailand (SAST), and the 90th Anniversary of Chulalongkorn University Fund (grant number GCUGR1125633048D) for financial support. Also, the authors would like to thank the Electrochemistry and Optical Spectroscopy Center of Excellence (EOSCE) and Department of Chemistry, Faculty of Science, Chulalongkorn University, for supporting the facilities that enable this study to be conducted.

Appendix A. Supplementary data

Supplementary data to this article can be found online at https://doi.org/10.1016/j.bios.2021.113387.

References

Ahmed, U., Anwar, A., Savage, R.S., Costa, M.L., Mackay, N., Filer, A., Raza, K., Watts, R. A., Winyard, P.G., Tarr, J., Haigh, R.C., Thornalley, P.J., Rabbani, N., 2015. Biomarkers of early stage osteoarthritis, rheumatoid arthritis and musculoskeletal health. Sci. Rep. 5, 9259.

Azevedo, V.H.R., da Silva, J.L., Stradiotto, N.R., 2019. Silver oxide nanoparticles in reduced graphene oxide modified electrode for amino acids electrocatalytic oxidation. J. Electroanal. Chem. 845, 57–65.

Babadi, F.E., Hosseini, S., Shavandi, A., Moghaddas, H., Shotipruk, A., Kheawhom, S., 2019. Electrochemical investigation of amino acids Parkia seeds using the composite electrode based on copper/carbon nanotube/nanodiamond. J. Environ. Chem. Eng. 7 (2), 102979.

Bi, Q., Dong, S., Sun, Y., Lu, X., Zhao, L., 2016. An electrochemical sensor based on cellulose nanocrystal for the enantioselective discrimination of chiral amino acids. Anal. Biochem. 508, 50–57.

Bianchi, V., Mazza, L., 1995. Rapid reversed-phase high-performance liquid chromatographic method with double derivatization for the assay of urinary hydroxyproline. J. Chromatogr. B Biomed. Appl. 665 (2), 295–302.

Bradbury, C.R., Kuster, L., Fermín, D.J., 2010. Electrochemical reactivity of HOPG electrodes modified by ultrathin films and two-dimensional arrays of metal nanoparticles. J. Electroanal. Chem. 646 (1), 114–123.

Chan, K.C., Janini, G.M., Muschik, G.M., Issaq, H.J., 1993. Micellar electrokinetic chromatography of hydroxyproline and other secondary amino acids in biological samples with laser-induced fluorescence detection. J. Chromatogr. 622 (2), 269–273.

Chen, C.Y., Wang, C.M., Chen, P.S., Liao, W.S., 2018. Self-standing aptamers by an artificial defect-rich matrix. Nanoscale 10 (7), 3191–3197.

Delport, M., Maas, S., van der Merwe, S.W., Laurens, J.B., 2004. Quantitation of hydroxyproline in bone by gas chromatography–mass spectrometry. J. Chromatogr. B 804 (2), 345–351.

Dong, Y.L., Yan, N., Li, X., Zhou, X.M., Zhou, L., Zhang, H.J., Chen, X.G., 2012. Rapid and sensitive determination of hydroxyproline in dairy products using micellar electrokinetic chromatography with laser-induced fluorescence detection. J. Chromatogr. A 1233, 156–160.

Feng, X., McDonald, J.M., 2011. Disorders of bone remodeling. Annu. Rev. Pathol. 6, 121–145.

Govindasamy, M., Wang, S.-F., Pan, W.C., Subramanian, B., Ramalingam, R.J., Al-lohedan, H., 2019. Facile sonochemical synthesis of perovskite-type SrTiO3 nanocubes with reduced graphene oxide nanocatalyst for an enhanced electrochemical detection of α-amino acid (tryptophan). Ultrason. Sonochem. 56, 193–199.

Jamall, I.S., Finelli, V.N., Que Hee, S.S., 1981. A simple method to determine nanogram levels of 4-hydroxyproline in biological tissues. Anal. Biochem. 112 (1), 70–75.

Jampasa, S., Siangproh, W., Duangmal, K., Chailapakul, O., 2016. Electrochemically reduced graphene oxide-modified screen-printed carbon electrodes for a simple and highly sensitive electrochemical detection of synthetic colorants in beverages. Talanta 160, 113–124.

Kontturi, M.J., Sotaniemi, E.A., Larmi, T.K., 1974. Hydroxyproline in the early diagnosis of bone metastases in prostatic cancer. Scand. J. Urol. Nephrol. 8 (2), 91–95.

Kotwal, A., Hurtado, M.D., Sfeir, J.G., Wermers, R.A., 2019. Transient osteoporosis: clinical spectrum IN adults and associated risk factors. Endocr. Pract. 25 (7), 648–656.

Li, H., Guan, H., Dai, H., Tong, Y., Zhao, X., Qi, W., Majeed, S., Xu, G., 2012. An amperometric sensor for the determination of benzophenone in food packaging materials based on the electropolymerized molecularly imprinted poly-o-phenylenediamine film. Talanta 99, 811–815.

Liang, H., Xue, J., Li, T., Wu, Y., 2005. A rapid capillary electrophoresis with electrochemiluminescence method for the assay of human urinary proline and hydroxyproline. Luminescence 20 (4–5), 287–291.

Luo, J., Huang, J., Cong, J., Wei, W., Liu, X., 2017. Double recognition and selective extraction of glycoprotein based on the molecular imprinted graphene oxide and boronate affinity. ACS Appl. Mater. Interfaces 9 (8), 7735–7744.

Messia, M.C., Di Falco, T., Panfili, G., Marconi, E., 2008. Rapid determination of collagen in meat-based foods by microwave hydrolysis of proteins and HPAEC-PAD analysis of 4-hydroxyproline. Meat Sci. 80 (2), 401–409.

Mujahid, A., Dickert, F.L., 2016. 5 - molecularly imprinted polymers: principle, design, and enzyme-like catalysis. In: Li, S., Cao, S., Piletsky, S.A., Turner, A.P.F. (Eds.), Molecularly Imprinted Catalysts. Elsevier, Amsterdam, pp. 79–101.

Ren, Y., Zhao, J., Shi, Y., Chen, C., Chen, X., Lv, C., 2017. Simple determination of L-hydroxyproline in idiopathic pulmonary fibrosis lung tissues of rats using non-extractive high-performance liquid chromatography coupled with fluorescence detection after pre-column derivatization with novel synthetic 9-acetylimidazol-carbazole. J. Pharmaceut. Biomed. Anal. 142, 1–6.

Russell, G., Mueller, G., Shipman, C., Croucher, P., 2001. Clinical disorders of bone resorption. Novartis Found. Symp. 232, 251–267 discussion 267-271.

Sakamoto, H., Watanabe, K., Koto, A., Koizumi, G., Satomura, T., Watanabe, S., Suye, S.-i., 2015. A bienzyme electrochemical biosensor for the detection of collagen l-hydroxyproline. Sens. Bio-Sens. Res. 4, 37–39.

Seibel, M.J., 2005. Biochemical markers of bone turnover: part I: biochemistry and variability. Clin. Biochem. Rev. 26 (4), 97–122.

Sheej Ahmad, O., 2018. Molecularly Imprinted Polymers in Electrochemical and Optical Sensors.

Shen, J., Gan, T., Jin, Y., Wang, J., Wu, K., 2018. Electrochemical sensor based on electropolymerized dopamine molecularly imprinted film for tetrabromobisphenol A. J. Electroanal. Chem. 826, 10–15.

Srivastava, A.K., Khare, P., Nagar, H.K., Raghuwanshi, N., Srivastava, R., 2016. Hydroxyproline: a potential biochemical marker and its role in the pathogenesis of different diseases. Curr. Protein Pept. Sci. 17 (6), 596–602.

Teerlink, T., Tavenier, P., Netelenbos, J.C., 1989. Selective determination of hydroxyproline in urine by high-performance liquid chromatography using precolumn derivatization. Clin. Chim. Acta 183 (3), 309–315.

Wasserman, H., O'Donnell, J.M., Gordon, C.M., 2017. Use of dual energy X-ray absorptiometry in pediatric patients. Bone 104, 84–90.

Woessner, J.F., 1961. The determination of hydroxyproline in tissue and protein samples containing small proportions of this imino acid. Arch. Biochem. Biophys. 93 (2), 440–447.

Xu, Y., Fang, L., Wang, E., 2009. Successful establishment of MEKC with electrochemiluminescence detection based on one functionalized ionic liquid. Electrophoresis 30 (2), 365–371.

Zheng, L., Zhao, X.E., Ji, W., Wang, X., Tao, Y., Sun, J., Xu, Y., Wang, X., Zhu, S., You, J., 2018. Core-shell magnetic molecularly imprinted polymers used rhodamine B hydroxyproline derivate as template combined with in situ derivatization for the specific measurement of L-hydroxyproline. J. Chromatogr. A 1532, 30–39.

Zhu, H., Yao, H., Xia, K., Liu, J., Yin, X., Zhang, W., Pan, J., 2018. Magnetic nanoparticles combining teamed boronate affinity and surface imprinting for efficient selective recognition of glycoproteins under physiological pH. Chem. Eng. J. 346, 317–328.